RSC Advances

PAPER

View Article Online
View Journal | View Issue

Cite this: *RSC Adv.*, 2023, **13**, 34587

Curcumin-loaded porous particles functionalized with pH-responsive cell-penetrating peptide for colorectal cancer targeted drug delivery

Zhila Izadi, *[ab] Maryam Rashidi,[bc] Hossein Derakhshankhah,[ab] Mozhdeh Dolati,[bc] Mohammad Ghanbari Kermanshahi,[ab] Hadi Adibi[a] and Hadi Samadian*[d]

The anticancer properties of curcumin have been broadly examined in several shapes, such as nanoparticles and nanocomposite structures. Despite its benefits, curcumin also has some disadvantages, including rapid metabolism, poor absorption, and rapid systemic excretion. Therefore, numerous strategies have been used to increase curcumin's bioavailability. One of these approaches is the use of porous particles like aerogels as drug carriers. Aerogels are special due to their peculiar physical structure. They have a high specific surface area, a significant amount of porosity, and a solid composition, which make them a good choice for drug delivery systems. In the present study, a pH-sensitive aerogel was constructed and evaluated for targeted drug delivery of curcumin to colon cancer. To control the release of curcumin, trehalose was used as a coating agent, and PLP (poly(L-lysine isophthalamide)) was used as a targeted drug delivery agent. PLP is a pseudo-peptidic polymer that increases the cell permeability. In order to investigate and compare the synthesized aerogel before and after loading curcumin and coating with trehalose, physicochemical characterization analyses were performed. Finally, the efficacy of the final formulation was evaluated on HT29 colon cells using the cell bioavailability test. The results indicated the successful synthesis of the aerogel with porous structure with solitary cavities. The trehalose coating performed well, preventing drug release at lower pH but allowing the drug to be released at its intended site. The designed curcumin-loaded porous particles functionalized with PLP showed significant efficacy due to increasing penetration of curcumin into cells, and has potential for use as a new drug carrier with dual effectivity in cancer therapy.

Received 14th September 2023
Accepted 21st September 2023

DOI: 10.1039/d3ra06270h

rsc.li/rsc-advances

Introduction

Colon cancer is one of the most common tumors worldwide and a leading cause of death.[1] Colon cancer is the second and third most common cancer among women and men, respectively.[2] Only 5% of cases of colorectal cancer are hereditary, and it most frequently develops spontaneously.[3,4] Surgery,[5] radiation therapy,[6] chemotherapy,[7] and targeted therapy can be used to treat colorectal cancer.[8] In recent years, with the advancement of nanotechnology, there has been great hope for the treatment of this cancer. As a growing branch of study, nanopharmaceutics is used to create and enhance new medications with greater efficacy.[9] A wide range of natural and therapeutic properties are known for the hydrophobic polyphenol curcumin, which is obtained from the rhizome of the herb *Curcuma longa*.[10] Curcumin, turmeric's active ingredient, has received a great deal of attention over the past two decades[11] due to its antioxidant,[12] anti-inflammatory,[13] antibacterial, and anti-carcinogenic properties.[14] The primary mechanism of action and cellular targets are based on literature data from experimental and clinical evaluation of curcumin in cancer therapy. In addition, recent advances in drug delivery systems for delivering curcumin to cancer cells are highlighted. Despite being effective and safe, curcumin's bioavailability has been cited as one of its main drawbacks.[15] The drawbacks of curcumin are listed as low serum levels,[16] restricted tissue distribution,[17] an apparent quick metabolism,[18] and a brief half-life.[19] To deal with these problems, modern drug delivery systems are recommended.[20] Controlling and encapsulating curcumin in a nano-carrier formulation can overcome these main disadvantages and possibly lead to improved efficacy.[21] In recent decades, advances in aerogel-related science have prompted increasing interest in these materials in pharmaceutical sciences for drug transport applications.[22] Their high surface area, porosity, and open pore structures that can be tuned and controlled by controlling the synthesis conditions make

[a]*Pharmaceutical Sciences Research Center, Health Institute, Kermanshah University of Medical Sciences, Kermanshah, Iran. E-mail: izadi_zh@razi.tums.ac.ir*
[b]*USERN Office, Kermanshah University of Medical Sciences, Kermanshah, Iran*
[c]*Student Research Committee, Kermanshah University of Medical Sciences, Kermanshah, Iran*
[d]*Research Center for Molecular Medicine, Hamadan University of Medical Sciences, Hamadan, Iran*

nanostructured aerogels promising materials for the conveyance of different drugs as well as chemicals and proteins.[23,24] Aerogels are the world's lightest processed solid substance with the highest percentage of space that is filled with gases in their structure.[25] A gel's liquid content is replaced with a gas to create an aerogel, per the definition.[26] Aerogels based on biopolymers such as polysaccharides,[27] proteins, and nucleic acids are the most widely investigated aerogels for biomedical applications.[28] One of the downsides of utilizing aerogels is that they can discharge drugs in an uncontrolled and rapid way after being administered, due to their huge surface area coming into contact with physiological media, particularly if the drug features high solvency and a high partition coefficient within the body's liquids.[29] However, specific coatings and incorporation of aerogels in other matrices, as well as regulation of the component's solubility, degree of crosslinking, functionalization, and interactions with the drug, can be used to enhance the ability of aerogels to function as platforms for controlled drug release.[30] Trehalose is one of the substances used for coating of aerogels.[31] A white crystalline disaccharide, trehalose is made up of two molecules of glucose joined by a 1,1-α-glycosidic bond.[32] The glycosidic bond that joins the two glucose units keeps trehalose in a closed-ring form.[33] Consequently, the aldehyde or the ketone ends cannot bind with lysine or arginine of proteins. Thus, trehalose is resistant to acid hydrolysis.[34] A new group of peptides known as cell-penetrating peptides (CPPs) has been characterized in recent years as a result of the identification and in-depth study of a number of peptides with the capacity to cross biological membranes.[35,36] PLP (poly(L-lysine isophthalamide)) is a CPP. Lysine-based CPP-mimetic polymers cause complete membrane disruption at late endosomal pH while remaining insoluble at physiological pH. The pH-dependent conformational changes and multivalent effects of their structures can effectively promote interaction with cell membranes, resulting in a significant increase in membranelytic activity compared to their linear counterparts. It was shown. The unique structure and pH-responsive cell-penetrating ability make novel polymers promising candidates for cytoplasmic delivery of biopolymer payloads.[37] The permeability of this material comes from its stringy structure, and it can create covalent bonds with other materials.[38]

Here, we designed a targeted drug delivery system with dual effectivity comprising curcumin-loaded porous particles functionalized with PLP pseudo-peptidic polymer and a coating of pH-responsive disaccharide. Starch polymer based-porous particles (aerogel) and PLP were synthesized. The fabricated aerogel was loaded with PLP as a permeability-increasing agent and curcumin as an anticancer agent. Finally, this carrier was coated with trehalose to improve the corrosion resistance, and its drug delivery performance in terms of drug loading capacity, drug discharge behavior, and cytotoxicity against cancerous cells was examined.

Materials

Curcumin (cur), L-lysine methyl ester hydrochloride, and isophthaloyl chloride were obtained from Sigma-Aldrich (St. Louis, MO, USA). Sodium azide (NaN_3), potassium bromide (KBr), hydrochloric acid (HCl), and solvents dimethyl sulfoxide (DMSO), diethyl ether, ethanol (EtOH), and acetone were obtained from Merck. Human colon cancer cell line (HT29) was purchased from the Iranian Biological Resource Center, and cell culture medium, fetal bovine serum (FBS), trypsin, and other cell culture supplements were provided by Gibco, Scotland.

Methods

Synthesis of poly(L-lysine isophthalamide) (PLP)

PLP was synthesized in accordance with the method reported by Eccleston *et al.*, using a single-phase polymerization technique.[38] In a conventional procedure, L-lysine methyl ester hydrochloride (5 mmol) and potassium carbonate (15 mmol) were dissolved in deionized water (10 ml). The aqueous solution was stirred using a Teflon-coated magnet at 25 °C and then cooled until an ice crystal was observed. A pre-cooled acetone solution (10 ml) containing isophthaloyl chloride (5 mmol) was rapidly added to the aqueous solution. The resulting solution reacted for 30 minutes, during which the poly L-lysine methyl ester hydrochloride precipitated into the solution (powdered cream white gum formed in 2–5 minutes). This resulting polymer was dried overnight in a vacuum oven at 60 °C. The dried poly L-lysine methyl ester was subsequently dissolved in a dimethyl sulfoxide solvent to prepare the sodium form of poly L-lysine isophthalamide. Following this, the same amount of 5% ethanol solution was slowly added to the polymer solution. The hydrolyzed polymer precipitated in 2–3 minutes and was then dissolved again in deionized water. The raw polymer solution was dialyzed in a dialysis system (passing through 10–12 kDa) against deionized water for about 2 days to remove unreacted and excess material. To obtain a neutral polymer, the polymer was acidified in sodium form to pH 3 using 1 M hydrochloric acid. The reaction is shown in Fig. 1A. Finally, the precipitate was collected, washed, and lyophilized to obtain a white powder. For the purpose of confirming and determining the structure of the synthesized PLP molecule, the NMR spectrum of PLP in d_6-DMSO was obtained using a Bruker Avance 500 MHz spectrometer at room temperature. Analysis of the molecular mass distribution was also performed using gel permeation chromatography (GPC).

Synthesis of aerogels

The aerogel base was made using the sol–gel technique. To start, 10 g of starch and 100 ml of distilled water were mixed and stirred for 24 hours to prepare a starch substrate. The substrate was then poured into a falcon and placed in the refrigerator overnight. Then, to remove water from the porous structure of the starch, it was placed in solutions with different percentages of ethanol. First, it was established in 50% ethanol for 24 hours, then in 70% ethanol for another 24 hours, and finally in 98% ethanol for 48 hours to form a stable and cohesive compound. Next, it was placed in the freezer for 24 hours and then dried in the freeze-dryer. After drying by freeze-dryer, the sample was ground with a mortar and then sieved.

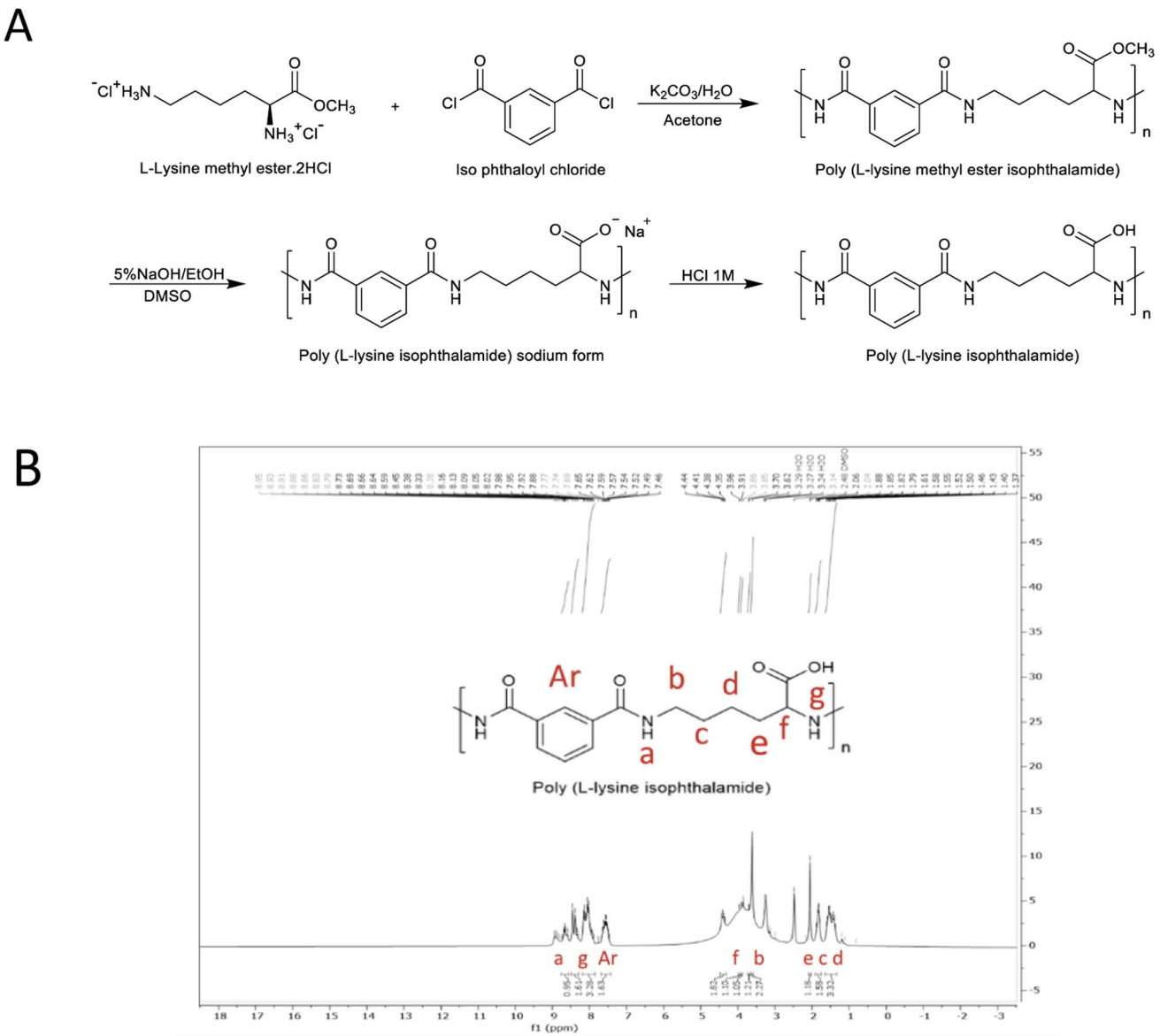

Fig. 1 Synthesis of poly L-lysine isophthalamide (PLP) using compression polymerization technique: (A) general schematic of synthetic steps towards amphiphilic poly L-lysine isophthalamide (PLP) pseudo-peptidic polymer using compression polymerization technique. (B) ^{1}H NMR (500 MHz) spectrum of synthesized PLP.

Loading of curcumin into aerogel particles and functionalization with PLP

The synthesized aerogel was initially mixed in a 1 : 1 ratio with 10 ml of acetone–ethanol solvent to load the aerogel with curcumin. The aerogel container was at that point filled with 20 mg of curcumin, and the reaction mixture was disturbed at 25 °C for 30 min. Then, after half an hour the synthetic PLP was added to the mixture. The sample was then allowed to slowly load for 48 hours while being incubated at 37 °C and 70 rpm, and then the material was centrifuged for 10 minutes at 8000 rpm. A spectrophotometer was used to measure the supernatant's adsorption in the 200–500 nm region using an acetone–ethanol blank. A homogeneous precipitate was produced by placing the precipitate first in the freezer to completely freeze, then in the freeze-dryer to completely dry the sample.

Coating of formulation

To coat the PLP-functionalized aerogel containing curcumin, trehalose and aerogel–Cur–PLP in an equal ratio were dissolved in water and placed in an incubator shaker for 48 hours to be coated at 37 °C and 70 rpm. The sample was centrifuged after 48 hours and dried again according to the conditions of the previous step.

Characterization

The structure of the synthesized compounds was examined with an FT-IR spectrometer (IR Prestige-21, Shimadzu Co., Japan) in the spectral range of 4000–400 cm^{-1} using a potassium bromide

disk at a resolution of 4 cm^{-1}. For the potassium bromide disk; 5–6 mg of sample was mixed and triturated with potassium bromide (100 mg) and placed in the sample holder. TGA was used to investigate changes in chemical and physical behavior of the aerogel, aerogel–Cur–PLP, and aerogel–Cur–PLP–Tre with temperature change, with a simultaneous thermal analyzer instrument (STA 503, BAHR, Germany). 10 mg of each sample was placed in an aluminum pan, and the temperature was raised to 700 °C at a ramp of 10 °C min^{-1} with air as the purge gas. The morphology of the aerogel was observed using a field emission scanning electron microscope (FEI Model Quanta 450 FEG, Hillsboro, OR, USA). The particle size of the resulting aerogel were analyzed using ImageJ software. At least 100 randomly selected samples obtained from different SEM images were analyzed for each sample. To assess the structure and morphology of the aerogel within the samples, an X-ray scattering test was performed by Philips X'Pert device (40 kV, 30 mA). To reach this goal, the samples were irradiated (Kα-Cu $\lambda =$ 1.54 A) at 2θ angles in the range of 20° to 80°. BET analysis was used to evaluate the specific surface area and porosity of the synthesized aerogel in the aerogel, aerogel–Cur–PLP, and also aerogel–Cur–PLP–Tre samples.

In vitro release study

A 10–12 kDa dialysis bag was cut to the appropriate size, one end was threaded, and 30 mg of the sample with 4 ml of 1 : 1 acetone–ethanol solvent was poured into the 10–12 kDa dialysis bag. It was placed in a container with 50 ml of phosphate buffer and dialyzed at pH 2.2, 5.5 and 7.4. The container was placed on a stirrer at room temperature and at predetermined time points 2 ml of buffer solution was removed to measure the amount of curcumin released, and 2 ml of phosphate was added to the buffer solution. The absorption of released curcumin at 430 nm was determined at different time intervals using a spectrophotometric device. The release rate is obtained using the equation:

$$\text{Release (LE\%)} = \frac{\text{weight of drug release}}{\text{the initial weight of drug added}}$$

In vitro cytotoxicity assay

The cytotoxic effects of curcumin and aerogel–Cur–PLP–Tre were examined using the 3-(4,5-dimethylthiazol-2-yl)-2,5-diphenyltetrazolium bromide (MTT) assay on a human colon cancer cell line (HT29). First, the cells were cultured in 96-well plates. The following day, different concentrations of curcumin and aerogel–Cur–PLP–Tre (0.0–160.0 μg ml^{-1}) were added to the wells, and the plates were incubated. After incubation time, MTT (5 mg ml^{-1}) was added to each well and the plates were then incubated for 3 h at 37 °C in 5% CO_2. Then, supernatants were removed and the reduced MTT dye was solubilized with DMSO. Absorbance was determined using an ELISA plate reader (Synergy H1 Hybrid Multi-Mode Microplate, Biotek, USA) with a test wavelength of 570 nm and a reference wavelength of 630 nm. The percent of viable cells for each concentration was calculated using the following formula:

$$\text{Viable cells (\%)} = \text{mean OD of the treatment wells/mean OD of the control wells} \times 100 \quad (1)$$

Subtracting these values from 100 gives us total cell growth inhibition, which is due to both the cytotoxic and anti-proliferative effects of the samples. The results are expressed as IC_{50} values.

Statistical analysis

The results are expressed as the mean values ± S.E. The comparison of multiple groups' means in functional *in vitro* studies was performed using the one-way ANOVA statistical test. Where the differences were significant, the Tukey test (Minitab software, version 18.1, SQC Institute, USA) was used. P values < 0.05 were considered statistically significant; $^*p < 0.05$.

Results and discussion

Proton nuclear magnetic resonance (^{1}H NMR) of PLP

The polymer PLP in acidic form was identified by ^{1}H NMR spectroscopy in d_6-DMSO solvent, as shown in Fig. 1B. Aliphatic CH_2 protons marked c, d, and e are visible in the 1–2 ppm region. Aliphatic CH_2 protons b and f appear in the 3.5 and 4.5 regions due to direct binding to nitrogen. The f protons are at higher field due to the direct connection of carbon to the C=O group. The protons of the aromatic ring and the NH of the amide group are also identified in the 7–9 ppm region.

Gel permeation chromatography (GPC) for PLP

The PLP molecular weight obtained in this study was 23.6 ± 5.61 kDa (Fig. 2). The standard polymer, polystyrene (PS), utilized in this analysis, is an exceedingly adaptable polymer without polar amide bunches, unlike PLP, which contains useful amphiphilic bunches and can form an organized structure. Subsequently, the atomic weight of PLP determined using the polystyrene standard cannot be a precise representation of the real atomic weight.

FT-IR spectroscopy analysis

The aerogel–Cur–PLP–Tre was synthesized *via* a reaction between the aerogel, curcumin, PLP, and trehalose. The structures and chemical grafting between each monomer of aerogel, curcumin, PLP, and trehalose were analyzed by FT-IR spectroscopy. The FT-IR spectrum of the synthesized aerogel is shown in Fig. 3. The peaks at 2933 and 2857 cm^{-1} corresponded to CH_2 and CH_3 symmetric and asymmetric stretching vibrations, respectively. The broad peak at 3406 cm^{-1} is a attributed to hydroxyl group (OH) stretching vibration, and the peaks at 1080 and 1016 cm^{-1} were related to the C–O stretching vibration of the cyclohexane monomer group of the starch. The presence of these peaks in the FT-IR spectrum of the aerogel confirmed the successful synthesis of the aerogel. Fig. 3 indicates the IR spectrum of the prepared aerogel–Cur–PLP. It shows characteristic peaks at 3429 cm^{-1} for the OH groups of the aerogel, PLP, and cur units. The CH_2 and CH_3 symmetric and asymmetric stretching vibrations of aerogel–Cur–PLP were

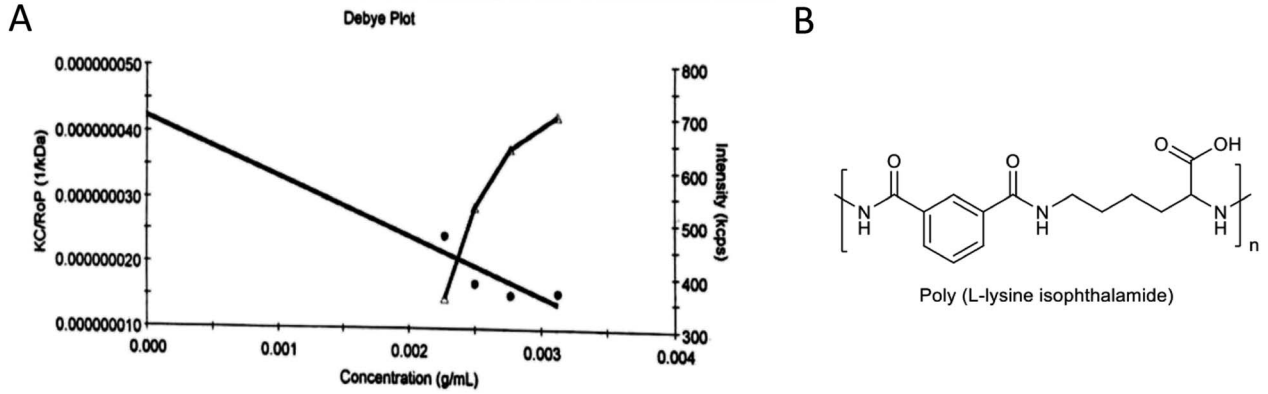

Fig. 2 (A) The molecular weight characterization results for PLP determined by gel permeation chromatography (GPC). (B) Chemical structure of amphiphilic PLP pseudo-peptidic polymer.

detected between 2862 and 2926 cm^{-1}. The absorption peaks at 3429 and 1639 cm^{-1} were attributed to N–H stretching and bending vibrations, respectively, and the absorption peak at 1242 cm^{-1} corresponds to the –C–N stretching vibration of the monomer PLP. The weak and sharp peaks at 3043 and 1654 cm^{-1}, respectively, correspond to the =C–H and C=C stretching vibrations of the double bonds of curcumin. The sharp peaks at 1732 and 1082 cm^{-1}, respectively, correspond to –C=O and –C–O, the carboxylic acid carbonyl stretching vibrations of the PLP and cur units. The peaks at 3429 and 1082 cm^{-1} correlate to OH and –C–O from the aerogel group, and the peaks at 2926 and 2826 cm^{-1} are a feature of the CH_2 and CH_3 symmetric and asymmetric stretching vibrations of the aerogel, confirming the synthesis of aerogel–Cur–PLP. Moreover, the presence of the peaks for PLP at 3429 cm^{-1} (attributed to N–H stretching vibration), 1639 cm^{-1} (attributed to N–H bending vibration), and 1242 cm^{-1} (corresponding to –C–N stretching vibration) and cur at 1732 cm^{-1} (corresponding to –C=O), 3043 cm^{-1} and 1654 cm^{-1} (corresponding to the =C–H and C=C stretching vibrations of the double bonds) confirmed the successful synthesis of aerogel–Cur–PLP. The FT-IR spectrum of the prepared aerogel–Cur–PLP–Tre (Fig. 3) indicated sharp peaks at 3404, 3040, 2926, 2854, 1647, 1635, 1568, 1463, 1431, 1236, 1155, 1082, and 1022 cm^{-1}; the absorption peaks at 3404 and 1635 cm^{-1} were attributed to N–H stretching and bending vibrations of monomer PLP, and the sharp peaks at 2924 and 2854 cm^{-1} are attributed to –C–H symmetric and asymmetric stretching vibrations. In the FT-IR spectrum of aerogel–Cur–PLP–Tre, there are peaks at 3043 and 1647 cm^{-1}, which correspond to C–H alkenes and aliphatic stretching vibration of the curcumin unit. The broad peak at 3404 cm^{-1} was attributed to OH stretching vibration group of carboxylic acid from curcumin and PLP units and hydroxyl from trehalose and aerogel. The sharp peaks at 1155 and 1082 cm^{-1}, respectively, correspond to stretching vibrations for C–O and the cyclohexyl ring of PLP. The presence of the peaks at 1647 and 3040 cm^{-1} correlates to C=C and =C–H from the curcumin group, and the peaks at 3404 and 1635 cm^{-1} are due to the N–H stretching and bending vibrations of the PLP, confirming the synthesis of aerogel–Cur–PLP–Tre. Furthermore, the FT-IR spectrum of aerogel–Cur–PLP–Tre showed prominent shifting of the peaks in comparison to those of aerogel–Cur–PLP. The peak positions were observed to change from 3429 to 3404, 1654 to 1647, 1639 to 1635, and 1047 to 1029 cm^{-1}. These results confirm the presence of aerogel–Cur–PLP and Tre in the spectrum of aerogel–Cur–PLP–Tre, and also the peaks in the spectrum of aerogel–Cur–PLP–Tre were detected at higher intensity peaks than the peaks of aerogel and aerogel–Cur–PLP.

Morphological assessment

The scanning electron microscopy (SEM) images of the aerogel are presented in Fig. 4; its structure is porous and contains single-handed cavities for loading into drug delivery systems. The aerogel has plant stem-like microstructures, which are disordered and randomly overlapping. The aerogel displayed honeycomb-ordered pores due to the sublimation of water. Furthermore, the average pore diameter of the aerogel was 19.78 μm and 17.03 μm, respectively, which can also be seen in the SEM images of the aerogel before and after loading curcumin, trehalose and PLP on the aerogel (Fig. 4). The aerogel seems to present ultrahigh porosity, ultralow density, and high elasticity. Thus, this aerogel can be used in drug loading and delivery.

Brunauer–Emmett–Teller (BET) analysis

The nitrogen adsorption and desorption isotherms of the aerogel before and after loading curcumin, PLP and trehalose coating are shown in Fig. 5A and B, along with their corresponding pore size distribution determined using the DH method. The specific surface area (S_{BET}), total pore volume (V_t) and pore size (W_{DH}) of the samples are given in Fig. 5C.

Determination of the crystallographic structure

According to the XRD diagram (Fig. 6A), the broad peak in the region of 20° indicates the amorphous and non-crystalline structure of the synthesized aerogel, and there was no change in this region even after the addition of curcumin and PLP. The process of forming an aerogel is associated with the loss of the granular crystalline structure of starch and its transformation into an amorphous aerogel structure. The crystalline state of the

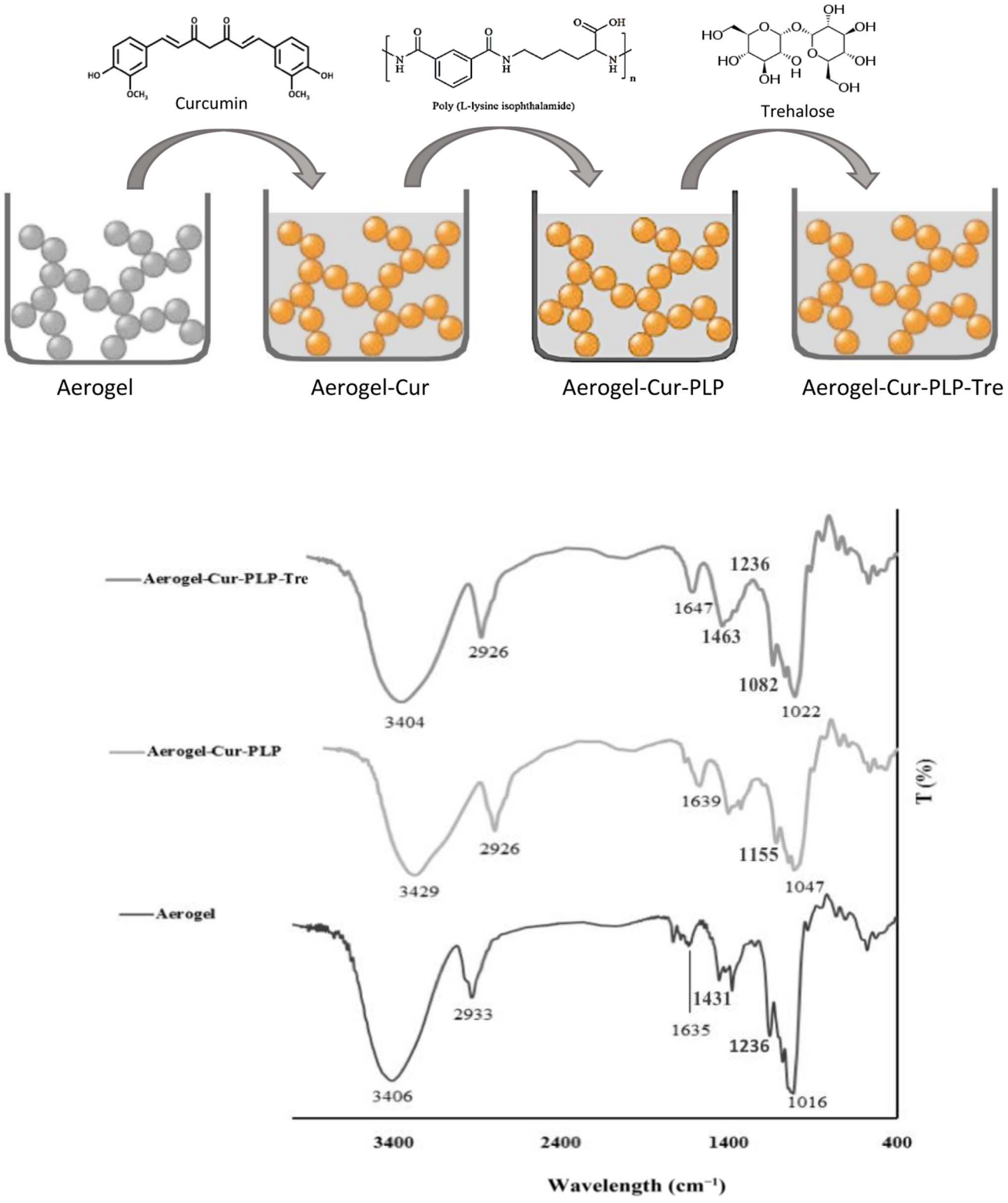

Fig. 3 The FT-IR spectra for aerogel, aerogel–Cur–PLP, and aerogel–Cur–PLP–Tre.

aerogel–Cur–PLP as well as the aerogel–Cur–PLP–Tre structures resulted in numerous and intense diffraction peaks that were visible in their spectra.

The thermal properties of the formulation

Fig. 6B shows the TGA curves for the dry aerogel, aerogel–Cur–PLP, and aerogel–Cur–PLP–Tre samples. First, the weight loss of

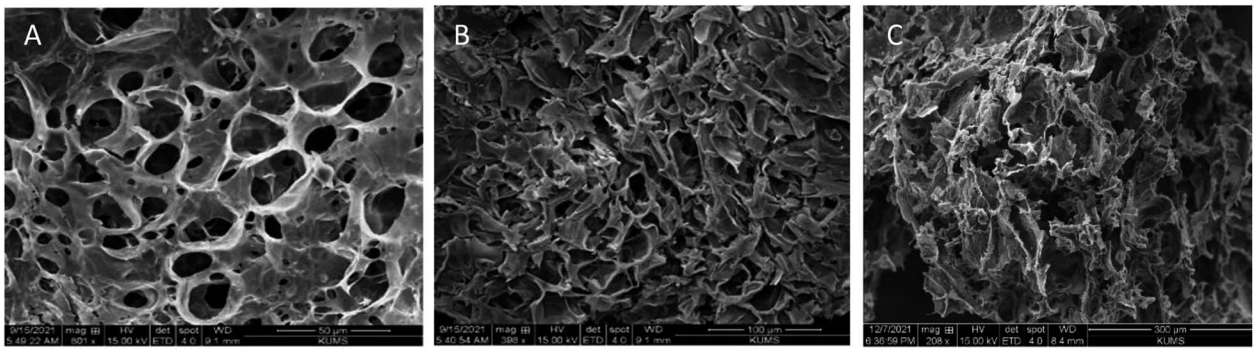

Fig. 4 SEM images of (A) aerogel, (B) aerogel–Cur–PLP, and (C) Aer–Cur–PLP–Tre under optimum conditions.

all samples, from 40 to 100 °C was ascribed to the loss of adsorbed and bound water in the structure of the samples. Aerogel degradation started at 305 °C and continued up to 360 °C, with 80% weight loss compared to the initial weight of the sample. The maximum decomposition temperature of the aerogel corresponded to 320 °C with a 52% weight loss compared to the initial weight of the sample. The aerogel–Cur–PLP thermogram included only one weight loss step. The degradation of aerogel–Cur–PLP occurred between 250 and 350 °C due to the removal of aerogel, Cur, and PLP. Over this temperature range, a weight loss of 55% was reported compared to the sample's initial weight. At the maximum decomposition temperature, which corresponds to 296 °C, a weight loss of 36% was reported compared to the sample's initial weight. The TGA thermograms show that the second step of aerogel–Cur–PLP–Tre degradation occurred between 270 and 360 °C. The degradation over this temperature range showed a weight loss of 75% compared to the sample's initial weight, due to the removal of the Tre monomer and PLP monomer as side chain. At the maximum decomposition temperature, which corresponds to 310 °C, a weight loss of 63% was reported compared to the sample's initial weight. Comparison of the TGA curves of aerogel–Cur–PLP–Tre, aerogel, and aerogel–Cur–PLP showed that the degradation of aerogel–Cur–PLP–Tre began at lower temperature and rate than those of aerogel–Cur–PLP. The thermal stability of aerogel–Cur–PLP–Tre is greater than that of aerogel–Cur–PLP, which is due to the physical entrapment of PLP in the aerogel–Cur–PLP–Tre core. Trehalose (owing to the OH bond) and PLP (owing to the C–O bond) have weak structures and decompose at low temperatures.

In vitro pH-responsive release study

In order to determine the release rate of curcumin from the aerogel synthesized with and without trehalose coating, it was investigated in three pH conditions of 2.2, 5.5 and 7.4 to

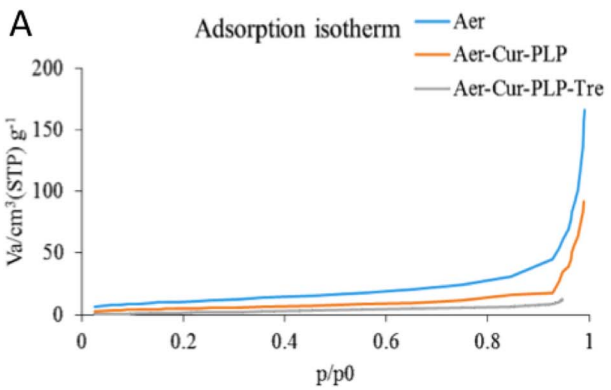

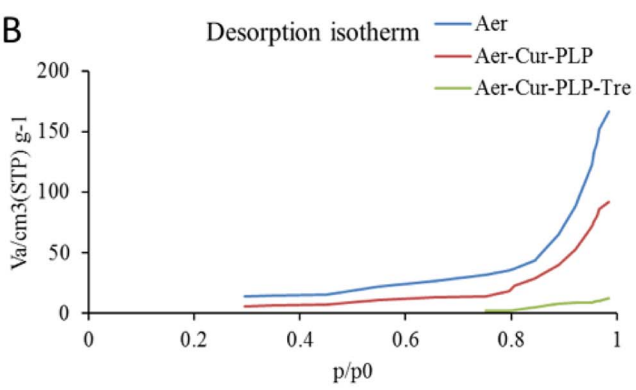

C

V_t (cm^3/g)	W_{DH} (nm)	S_{BET} (m^2/g)	sample
0.2531	25.432	39.81	Aer
0.1415	30.763	18.399	Aer-Cur-PLP
0.019064	9.1197	8.3617	Aer-Cur-PLP-Tre

Fig. 5 The result of BET analysis: (A) nitrogen adsorption and (B) desorption isotherms of the aerogel before and after curcumin loading and trehalose coating. (C) Structural characteristics of aerogel pores, before and after loading curcumin and coating with trehalose.

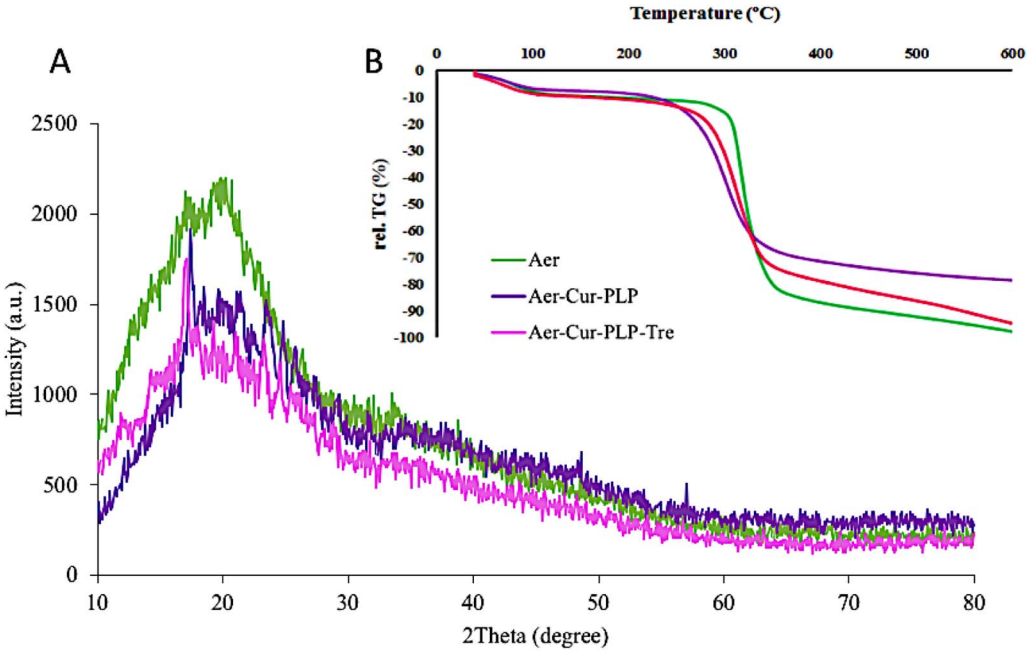

Fig. 6 The (A) X-ray diffraction (XRD) and (B) TGA results for Aer, Aer–Cur–PLP, and Aer–Cur–PLP–Tre.

simulate the digestive system. The absorption of the samples was taken using a spectrophotometric device and by placing them in the equation of the calibration curve, the amount of curcumin released in all three simulated conditions was obtained. Fig. 7 shows that the curcumin is released from all samples in the first 420 minutes. According to Fig. 7A, which shows the results for the sample without trehalose coating, the percentages of curcumin released are not much different and no control has been exercised over the release of curcumin, but according to Fig. 7B, which is associated with the trehalose coating, the release of curcumin is controlled by the trehalose coating agent. Due to the pH-responsive feature of trehalose, curcumin is not released in large quantities under acidic conditions, whereas it is released quite differently under neutral pH conditions. Considering these two diagrams and comparing them with each other, it can be concluded that trehalose has acted successfully as a coating agent that has the task of controlling the release of curcumin at different pHs. Actually, the glycosidic bond that joins the two glucose units keeps trehalose in a closed-ring form. Consequently, the aldehyde or the ketone ends cannot bind with lysine or arginine of proteins. Thus, trehalose is resistant in acidic pH. Considering the steady and uniform permeable structure, tunable pore sizes, expanded surface region, and surface properties of permeable materials, and great progress has been made in developing permeable biopolymers for controlled drug delivery. The trehalose, PLP, and starch aerogel-based pH-sensitive drug delivery system has increased selectivity toward cancer cells through reacting to the inside stimulus (pH) and outside stimulus. The significance of pH-responsive carriers for the treatment of cancer is related to the more acidic pH of the tumor tissue environment. The aerogel–Cur–PLP–Tre carrier can be utilized to discharge the drug into the acidic tumor tissue, given that the solubility of PLP increases in acidic situations owing to the protonation of amine bunches.

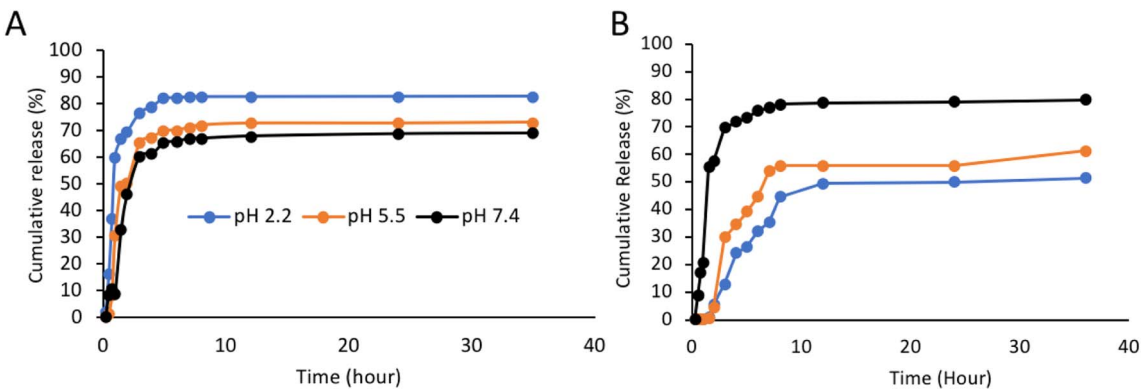

Fig. 7 Comparison of curcumin release from aerogel (A) without trehalose coating and (B) with trehalose coating at pH 2.2, 5.5 and 7.4.

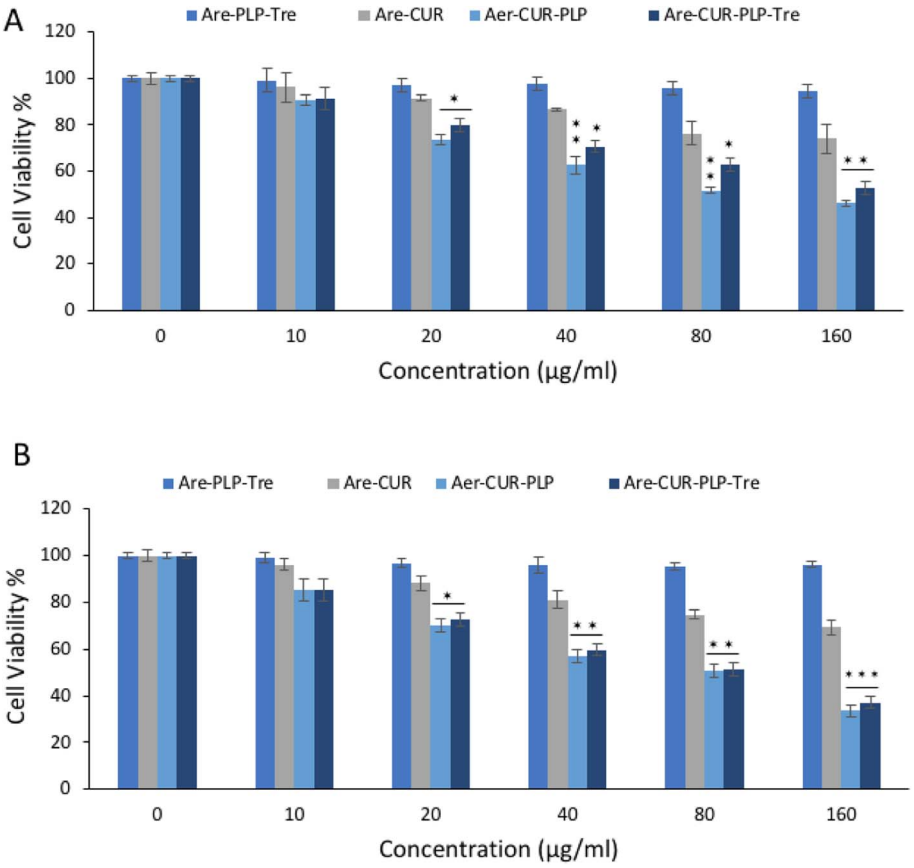

Fig. 8 The results of MTT assay for cytotoxicity of aerogel–Cur–PLP–Tre and curcumin on HT29 cells line after (A) 24 and (B) 48 h of incubation.

In vitro cytotoxicity study

The anti-proliferative effect of aerogel–Cur–PLP–Tre on HT29 cell lines was investigated and compared with that of free curcumin on these cells by MTT assay. The results are reported in Fig. 8; a more cytotoxic effect on HT29 cell lines was observed with aerogel–Cur–PLP–Tre in comparison to the control experiment with free curcumin in the same concentration range. The IC_{50} values obtained for aerogel–Cur–PLP–Tre and free curcumin in HT29 cells were 49 and 80 μg ml^{-1} (after 24 h of incubation), and 37 and 68 μg ml^{-1} (after 48 h of incubation), respectively. The obtained results strongly suggest that aerogel–Cur–PLP–Tre is an ideal drug delivery vehicle that could significantly enhance the pharmacodynamics of curcumin.

Conclusion

The special qualities of aerogels bring new ways to solve pertinent drug formulation problems and create sophisticated drug delivery systems with novel capabilities. Large amounts of drugs in an amorphous state can be deposited on the aerogel skeleton to make up for poor drug solubility. The extensive pore network and wide surface area make it easier for the dissolved medication to diffuse into the aqueous environment. Aerogels can be synthesized in different shapes and surface properties, making them adaptable to various applications. Polysaccharide aerogels, such as starch, are attractive candidates as vectors for drug delivery because of their biocompatibility and biodegradability, porous structure, huge surface area and ability to load drugs. Essentially, this work highlights the potential to regulate drug loading and release kinetics by selecting appropriate polysaccharide-based aerogels. According to the obtained results, the coating of curcumin by trehalose, which causes resistance to acidic conditions, as well as the use of PLP to increase the colon cell membrane permeability, provides a suitable drug delivery system for the treatment of colon cancer.

Conflicts of interest

Declared none.

Acknowledgements

This research was financially supported by the Kermanshah University of Medical Sciences (KUMS), No. 990727.

References

1 T. A. Baudino, Targeted cancer therapy: the next generation of cancer treatment, *Curr. Drug Discovery Technol.*, 2015, **12**(1), 3–20.
2 J. Erdrich, X. Zhang, E. Giovannucci and W. Willett, Proportion of colon cancer attributable to lifestyle in

a cohort of US women, *Cancer Causes Control*, 2015, **26**(9), 1271–1279.
3 S. J. O'keefe, Diet, microorganisms and their metabolites, and colon cancer, *Nat. Rev. Gastroenterol. Hepatol.*, 2016, **13**(12), 691–706.
4 V. Gianfredi, T. Salvatori, M. Villarini, M. Moretti, D. Nucci and S. Realdon, Is dietary fibre truly protective against colon cancer? A systematic review and meta-analysis, *Int. J. Food Sci. Nutr.*, 2018, **69**(8), 904–915.
5 S. Tohme, R. L. Simmons and A. Tsung, Surgery for cancer: a trigger for metastases, *Cancer Res.*, 2017, **77**(7), 1548–1552.
6 D. Schaue and W. H. McBride, Opportunities and challenges of radiotherapy for treating cancer, *Nat. Rev. Clin. Oncol.*, 2015, **12**(9), 527–540.
7 A. D. Wagner, N. L. Syn, M. Moehler, W. Grothe, W. P. Yong, B. C. Tai and et al., Chemotherapy for advanced gastric cancer, *Cochrane Database Syst. Rev.*, 2017, **8**, 29–42.
8 S. Chakrabarti, C. Y. Peterson, D. Sriram and A. Mahipal, Early stage colon cancer: current treatment standards, evolving paradigms, and future directions, *World J. Gastrointest. Oncol.*, 2020, **12**(8), 808.
9 L. Kotelevets, E. Chastre, D. Desmaele and P. Couvreur, Nanotechnologies for the treatment of colon cancer: from old drugs to new hope, *Int. J. Pharm.*, 2016, **514**(1), 24–40.
10 R. K. Verma, P. Kumari, R. K. Maurya, V. Kumar, R. Verma and R. K. Singh, Medicinal properties of turmeric (Curcuma longa L.): a review, *Int. J. Chem. Stud.*, 2018, **6**(4), 1354–1357.
11 S. J. Hewlings and D. S. Kalman, Curcumin: a review of its effects on human health, *Foods*, 2017, **6**(10), 92.
12 M. M. Yallapu, P. K. B. Nagesh, M. Jaggi and S. C. Chauhan, Therapeutic applications of curcumin nanoformulations, *AAPS J.*, 2015, **17**(6), 1341–1356.
13 K. M. Nelson, J. L. Dahlin, J. Bisson, J. Graham, G. F. Pauli and M. A. Walters, The essential medicinal chemistry of curcumin: miniperspective, *J. Med. Chem.*, 2017, **60**(5), 1620–1637.
14 B. Salehi, Z. Stojanović-Radić, J. Matejić, M. Sharifi-Rad, N. V. A. Kumar, N. Martins and et al, ., The therapeutic potential of curcumin: a review of clinical trials, *Eur. J. Med. Chem.*, 2019, **163**, 527–545.
15 R. R. Kotha and D. L. Luthria, Curcumin: biological, pharmaceutical, nutraceutical, and analytical aspects, *Molecules*, 2019, **24**(16), 2930.
16 S.-I. Sohn, A. Priya, B. Balasubramaniam, P. Muthuramalingam, C. Sivasankar, A. Selvaraj and et al, ., Biomedical applications and bioavailability of curcumin—an updated overview, *Pharmaceutics*, 2021, **13**(12), 2102.
17 N. Ahangari, S. Kargozar, M. Ghayour-Mobarhan, F. Baino, A. Pasdar, A. Sahebkar and et al, ., Curcumin in tissue engineering: a traditional remedy for modern medicine, *BioFactors*, 2019, **45**(2), 135–151.
18 C. Schneider, O. N. Gordon, R. L. Edwards and P. B. Luis, Degradation of curcumin: from mechanism to biological implications, *J. Agric. Food Chem.*, 2015, **63**(35), 7606–7614.
19 M. Dei Cas and R. Ghidoni, Dietary curcumin: correlation between bioavailability and health potential, *Nutrients*, 2019, **11**(9), 2147.
20 D. Shah, R. Savaliya, P. Patel, K. Kansara, A. Pandya, A. Dhawan and et al, ., Curcumin Ag nanoconjugates for improved therapeutic effects in cancer, *Int. J. Nanomed.*, 2018, **13**, 75.
21 P. Sivasami and T. Hemalatha, Augmentation of therapeutic potential of curcumin using nanotechnology: current perspectives, *Artif. Cells, Nanomed., Biotechnol.*, 2018, **46**(suppl. 1), 1004–1015.
22 L. Zheng, S. Zhang, Z. Ying, J. Liu, Y. Zhou and F. Chen, Engineering of aerogel-based biomaterials for biomedical applications, *Int. J. Nanomed.*, 2020, **15**, 2363.
23 J. Stergar and U. Maver, Review of aerogel-based materials in biomedical applications, *J. Sol-Gel Sci. Technol.*, 2016, **77**(3), 738–752.
24 L. E. Nita, A. Ghilan, A. G. Rusu, I. Neamtu and A. P. Chiriac, New trends in bio-based aerogels, *Pharmaceutics*, 2020, **12**(5), 449.
25 C. Ziegler, A. Wolf, W. Liu, A. K. Herrmann, N. Gaponik and A. Eychmüller, Modern inorganic aerogels, *Angew. Chem., Int. Ed.*, 2017, **56**(43), 13200–13221.
26 I. Smirnova and P. Gurikov, Aerogel production: current status, research directions, and future opportunities, *J. Supercrit. Fluids*, 2018, **134**, 228–233.
27 K. Ganesan, T. Budtova, L. Ratke, P. Gurikov, V. Baudron, I. Preibisch and et al, ., Review on the production of polysaccharide aerogel particles, *Materials*, 2018, **11**(11), 2144.
28 H. Maleki, L. Durães, C. A. García-González, P. Del Gaudio, A. Portugal and M. Mahmoudi, Synthesis and biomedical applications of aerogels: possibilities and challenges, *Adv. Colloid Interface Sci.*, 2016, **236**, 1–27.
29 C. A. García-González, A. Sosnik, J. Kalmár, I. De Marco, C. Erkey, A. Concheiro and et al, ., Aerogels in drug delivery: from design to application, *J. Controlled Release*, 2021, **332**, 40–63.
30 T. A. Esquivel-Castro, M. Ibarra-Alonso, J. Oliva and A. Martínez-Luévanos, Porous aerogel and core/shell nanoparticles for controlled drug delivery: a review, *Mater. Sci. Eng., C*, 2019, **96**, 915–940.
31 C. Olsson, H. Jansson and J. Swenson, The role of trehalose for the stabilization of proteins, *J. Phys. Chem. B*, 2016, **120**(20), 4723–4731.
32 C. M. Figueroa and J. E. Lunn, A tale of two sugars: trehalose 6-phosphate and sucrose, *Plant Physiol.*, 2016, **172**(1), 7–27.
33 X. Cai, I. Seitl, W. Mu, T. Zhang, T. Stressler, L. Fischer and et al, ., Biotechnical production of trehalose through the trehalose synthase pathway: current status and future prospects, *Appl. Microbiol. Biotechnol.*, 2018, **102**(7), 2965–2976.
34 S. Jana and S. S. Kulkarni, Synthesis of trehalose glycolipids, *Org. Biomol. Chem.*, 2020, **18**(11), 2013–2037.

35 G. Guidotti, L. Brambilla and D. Rossi, Cell-penetrating peptides: from basic research to clinics, *Trends Pharmacol. Sci.*, 2017, **38**(4), 406–424.
36 J. D. Ramsey and N. H. Flynn, Cell-penetrating peptides transport therapeutics into cells, *Pharmacol. Ther.*, 2015, **154**, 78–86.
37 K. A. Watkins and R. Chen, pH-responsive, lysine-based hydrogels for the oral delivery of a wide size range of molecules, *Int. J. Pharm.*, 2015, **478**(2), 496–503.
38 M. E. Eccleston, N. K. Slater and B. J. Tighe, Synthetic routes to responsive polymers; co-polycondensation of tri-functional amino acids with diacylchlorides, *React. Funct. Polym.*, 1999, **42**(2), 147–161.